PHYSICAL REVIEW C **85**, 054609 (2012)

High resolution spectroscopy of ^{112}Sn through the ^{114}Sn(p,t)^{112}Sn reaction

P. Guazzoni,[1] L. Zetta,[1] A. Covello,[2,3] A. Gargano,[3] B. F. Bayman,[4] G. Graw,[5] R. Hertenberger,[5] H.-F. Wirth,[5]
T. Faestermann,[6] and M. Jaskóla[7]
[1]*Dipartimento di Fisica dell'Università, and Istituto Nazionale di Fisica Nucleare, Via Celoria 16, I-20133 Milano, Italy*
[2]*Dipartimento di Scienze Fisiche, Università di Napoli Federico II, Complesso Universitario di Monte S. Angelo,*
Via Cintia, I-80126 Napoli, Italy
[3]*Istituto Nazionale di Fisica Nucleare, Complesso Universitario di Monte S. Angelo, Via Cintia, I-80126 Napoli, Italy*
[4]*School of Physics and Astronomy, University of Minnesota, Minneapolis, Minnesota 55455, USA*
[5]*Fakultät für Physik der LMU, D-85748 Garching, Germany*
[6]*Physik Department TUM, D-85748 Garching, Germany*
[7]*Soltan Institute for Nuclear Studies, Warsaw, Poland*

(Received 21 March 2012; published 7 May 2012)

The ^{114}Sn(p,t)^{112}Sn reaction has been investigated in a high resolution experiment at incident proton energy of 22 MeV. Angular distributions for 28 transitions to levels of ^{112}Sn up to the excitation energy of 3.624 MeV have been measured. The spin and parity identification has been carried out by means of a distorted-wave Born approximation (DWBA) analysis, performed by using conventional Woods-Saxon potentials. A shell-model study of ^{112}Sn nucleus has been performed using a realistic two-body effective interaction derived from the CD-Bonn nucleon-nucleon potential. The energy spectra have been calculated and compared with the experimental ones, while the theoretical two-nucleon spectroscopic amplitudes, evaluated in a truncated seniority space, have been used in the microscopic DWBA calculation of the cross-section angular distributions.

DOI: 10.1103/PhysRevC.85.054609 PACS number(s): 25.40.Hs, 21.10.Hw, 21.60.Cs, 27.60.+j

I. INTRODUCTION

Transfer reactions with light particles, investigated in high resolution experiments, represent a unique and very important source of information on nuclear structure near closed shells. In particular, the two-neutron transfer reactions are very sensitive probes for studying pairing correlations in the overlap between initial and final states. Therefore, as a specific probe of this type of correlations, the (p,t) reactions play a crucial role both in the study of the low-spin states of nuclei and in the test of the relative phases of spectroscopic amplitudes provided by the shell model. The two-neutron transfer data may be integrated with those coming from other nuclear reactions, each one characterized by its specific selectivity in the population of the excited states. In this way, the complete level scheme up to a certain spin and excitation energy, as well as evidence for different excitation modes, can be obtained.

The tin isotopic chain, with 10 stable isotopes from ^{112}Sn to ^{124}Sn, provides a very good opportunity for such detailed studies near the $Z = 50$ closed shell. In this case, one may assume that only the five neutron orbitals $0g_{7/2}$, $1d_{5/2}$, $1d_{3/2}$, $2s_{1/2}$, and $0h_{11/2}$ of the 50-82 shell contribute to the low-lying excitations. The investigation of the interplay and mixing of configurations arising from these orbitals, as well as of the limits of this description, requires a large amount of experimental data concerning both low-spin and high-spin states. The linked use of different techniques, such as γ-ray spectroscopy, with both selective and nonselective reactions, β decay, elastic and inelastic scattering, and transfer reactions, may help to achieve this aim.

In recent years, we have performed a systematic study of tin isotopes via (p,t) reactions in high resolution experiments at the Munich HVEC MP Tandem. We reported the results for ^{112,116,118,120,122,124}Sn(p,t)^{110,114,116,118,120,122}Sn reactions in previous papers [1–5], where they were also compared with predictions of shell-model calculations. The present paper, devoted to the measurement and analysis of the ^{114}Sn(p,t)^{112}Sn reaction, completes our study of even tin isotopes.

Fleming *et al.* [6] performed a study of several even Sn isotopes at an incident energy of 20 MeV, with an energy resolution of 25 keV. In the ^{114}Sn(p,t)^{112}Sn reaction only the transitions to the ground state, first excited 2^+ state, and first excited 3^- state were identified. A ^{114}Sn(p,t)^{112}Sn experiment with a resolution of about 14 keV was performed by Blankert [7] at a proton energy of 27.5 MeV. Levels up to 4.4 MeV of excitation energy were observed and L values were determined up to 3.5 MeV of excitation energy, but these results were never published.

On these grounds, we have undertaken a new study of the ^{114}Sn(p,t)^{112}Sn reaction at incident proton energy of 22 MeV, carrying out a high resolution experiment to characterize the low-spin states of ^{112}Sn.

The excited states of ^{112}Sn have been studied by a variety of methods, that can be summarized as follows:

(i) Measurements of the energies of γ rays following the β^+ decay of ^{112}Sb [9] and populating many low-lying states.
(ii) ^{100}Mo(^{16}O,4$n\gamma$) studies [10], which have identified distinct deformed bands on the high-spin region of ^{112}Sn as those of the proton intruder configuration. Using the same reaction [11] the lifetimes of $J^\pi = 8^-$ and $J^\pi = 9^-$ states have been measured and a large $BE(2)$ value, $(175 \pm 35)e^2$ fm^4, has been obtained for the $9^- \rightarrow 8^-$ transition in ^{112}Sn.

(iii) 0^+ states have been observed with the two-proton transfer reaction ^{110}Cd(^{3}He,n) at 25.4 MeV [12].

(iv) A nanosecond isomer in ^{112}Sn has been investigated using the reaction ^{112}Cd(^{3}He,$3n$) at 29 MeV [13]. The half-life of the $J^\pi = 6^+$ 2548.9 keV level [(13.8 ± 0.4) ns] and the $B(E2, 6_1^+ \rightarrow 4_1^+)$ (0.49 W.u.) have been obtained.

(v) ^{110}Cd(α,$2n\gamma$)^{112}Sn studies have identified collective bands associated with 2p-2h excitation [14] as well as high-spin neutron quasiparticle excitations [15] up to levels with $J^\pi = 12^+$. The measurements included γ-ray excitation functions, γ-γ coincidences, lifetimes, γ-ray angular distributions, γ-ray linear polarization, and conversion electron measurements.

(vi) $0^+, 2^+, 4^+$, and 3^- states have been investigated [16,17] via (^{16}O,^{16}O$'\gamma$) Coulomb excitation measurements. $B(E2)$ transition probabilities between these levels have been obtained as well as the $B(E3; 0_1^+ \rightarrow 3_1^-)$.

(vii) Inelastic scattering of protons [16,18].

(viii) (p,t) transfer reactions [6,7].

The results obtained in the studies mentioned above for ^{112}Sn are reported in the Nuclear Data Sheets (NDS) compilations [8], where a more complete list of references can be found.

In order to gain a better insight into the structure of ^{112}Sn, the present experimental data have been supplemented by distorted-wave Born approximation (DWBA) microscopic calculations of differential cross sections for the ground state and the observed excited states of ^{112}Sn. The two-neutron spectroscopic amplitudes obtained by shell-model calculations for the ^{114}Sn target and ^{112}Sn residual nucleus have been used. These calculations have been performed within the framework of the seniority scheme using a realistic effective interaction derived from the CD-Bonn nucleon-nucleon potential [20]. The model space has been truncated to states with seniority less than or equal to 4, to reduce the numerical work required by a complete-basis diagonalization. However, a full shell-model study of both positive- and negative-parity spectra of ^{112}Sn has been also performed.

An outline of the experimental method and analyzing procedure is given in Sec. II. In Sec. III the theoretical framework of shell-model calculation is described and the experimental and theoretical energy spectra of ^{112}Sn are compared. In Sec. IV the microscopic DWBA calculations of the differential cross sections are presented. Section V contains a summary of our conclusions.

II. EXPERIMENTAL METHOD AND ANALYZING PROCEDURE

A. The experiment

The ^{114}Sn(p,t)^{112}Sn reaction has been studied by using the 22 MeV proton beam delivered by the HVEC MP Tandem accelerator of the Maier-Leibnitz Laboratory of the Ludwig Maximilians University and Technical University of Munich. The beam current intensity ranged from 300 to 500 nA to avoid target heating and was integrated into a Faraday cup set behind the target, allowing measurements of absolute differential cross sections.

The reaction products were momentum separated and analyzed with the Munich Q3D spectrograph [21] and then detected in its focal plane at 8 angles from $\theta = 10^\circ$ to $\theta = 57.5^\circ$ with respect to the beam axis in 4 different magnetic field settings, reaching an excitation energy of the ^{112}Sn residual nucleus of 3.624 MeV. The magnetic field values have been set to allow overlaps in energy.

The acceptance opening of the magnetic spectrograph was 11.04 msr (slits of 20 mm horizontally, 20 mm vertically). The tritons emitted in the ^{114}Sn(p,t)^{112}Sn reaction were identified by the 1 m long focal plane detector [22] designed to detect light ions such as p, d, t, ^{3}He, and alpha with a position resolution better than 0.1 mm, good particle identification, and high count rate. The focal plane detector consists of a position-sensitive proportional counter with cathode strip readout and a 7 mm thick plastic scintillator (Ne-104). The photomultiplier signal together with the wire signals allowed the particle identification. Because of the excellent separation of the tritons from other reaction products, the measured spectra are virtually free from the contamination of other particles. The spectrograph is an ideal instrument for measuring transfer reactions. The very good energetic characteristics of the accelerator, the Q3D, and the detector enable us to measure high resolution excitation spectra with an energy resolution of about 8 keV full width at half maximum in the detection of the outgoing tritons.

The thickness of the ^{114}Sn target used is 113 μg/cm^2 on a carbon backing of 10 μg/cm^2. The low available isotopic enrichment (71%) of the ^{114}Sn target deserves special attention, because of the presence of some kind of discontinuous "background" arising from the contribution of other abundant tin isotopes (*contaminants*) present in the target. This presence, even if it can be a useful tool in the spectrum energy calibration, has the disadvantage of contaminating some of the transitions to the final nucleus ^{112}Sn. In order to allow safe identification of the residual nucleus ^{112}Sn level energies and correct evaluation of the differential cross sections, a natural tin target Sn$_{\text{nat}}$ (thickness 127 μg/cm^2 on a carbon backing of 10 μg/cm^2) was also used in the experiment, as reference. In Table I the isotopic composition of the ^{114}Sn target is reported together with the isotopic composition of the natural tin. The spectra from both ^{114}Sn and Sn$_{\text{nat}}$ targets were recorded at each angle of each magnetic field setting. In fact, we can consider that in the ^{114}Sn target used there are two different classes of contaminants. To the first class belong the transitions that fall between two contiguous levels of ^{112}Sn, useful also for the energy calibration, as previously said. To the second class belong the transitions that are superimposed to a level of ^{112}Sn. The knowledge of the isotopic composition of the ^{114}Sn target allows to neglect the peaks arising from the first-class contaminants. The knowledge of the isotopic composition of

TABLE I. Target isotopic composition percentages

Target	112	114	115	116	117	118	119	120	122	124
^{114}Sn	0.27	71.1	0.77	10.23	2.45	6.30	1.78	5.89	0.60	0.61
Sn$_{\text{nat}}$	1.0	0.7	0.4	14.7	7.7	24.3	8.6	32.4	4.6	5.6

the Sn$_{\mathrm{nat}}$ target and the measurement of its spectra at each angle allows to correctly evaluate the contribution of the second-class contaminants. Furthermore it has to be noted that in the Sn$_{\mathrm{nat}}$ target the percentage of ^{114}Sn is only 0.7%. Thus peaks belonging to ^{112}Sn are practically absent in the triton spectra from this target.

The energy calibration of the collected spectra was carried out by measuring, in the same magnetic conditions, spectra from the ^{116}Sn(p,t)^{114}Sn reaction, using a 98.0% enriched target. This choice is due to several reasons. ^{116}Sn is the most abundant contaminant in our ^{114}Sn target, and the Q-value difference between the ^{116}Sn(p,t)^{114}Sn reaction, already measured by us [2], and the ^{114}Sn(p,t)^{112}Sn reaction, is only 933 keV.

The ^{114}Sn energy calibration has been done using the γ-decay energies [19]. The correlation between the measured channels and the excitation energies was established using a polynomial of rank 2. The polynomial coefficients were fixed in each measured energy range by imposing the reproduction of the adopted energies. The polynomial coefficients obtained from each spectrum of the ^{116}Sn(p,t)^{114}Sn reaction were used to calibrate the energy spectra of both ^{114}Sn(p,t)^{112}Sn, and (from the Sn$_{\mathrm{nat}}$ target) the ^{A}Sn(p,t)$^{A-2}$Sn reactions. In addition the ^{112}Sn energy calibration was verified using γ-decay energies for ^{112}Sn [8]. The fitting procedure of triton spectra was carried out with the AUTOFIT shape-fitting code [23] using as reference the shape of a proper triton peak for each magnetic setting.

In Fig. 1 triton position spectra collected at $\theta_{\mathrm{lab}} = 20^\circ$ are shown. Figure 1(a) shows the triton position spectrum as collected on beam from the ^{114}Sn target at several magnetic settings. Due to the presence of the other tin isotopes in the target, many levels, coming from the (p,t) reactions on all the others tin isotopes, are visible. In the triton position spectrum of Fig. 1(b), only the transitions to the ^{112}Sn residual nucleus, as obtained by "properly subtracting" the contaminant contribution, are shown. In both Figs. 1(a) and 1(b) the arrows (portions α and γ, respectively) indicate the part of the spectrum corresponding to the second collected magnetic setting. Figure 1(c) reports the position spectra (α and γ) corresponding to the second magnetic setting for Fig. 1(a) and Fig. 1(b), while the β spectrum is due to the tritons coming from the Sn$_{\mathrm{nat}}$ target, obviously collected with the same magnetic setting. For the sake of simplicity, in Fig. 1 only some levels are labeled with their excitation energy in MeV. Except for ^{112}Sn, the residual nuclei are indicated with their mass number.

By considering Fig. 1, it is possible to have an idea of the procedure followed in the analysis of the experimental data, i.e., how to "clean" the on-beam collected position spectra from the presence of the tritons coming from the (p,t) reactions on the contaminating isotopes of the ^{114}Sn target. First of all, as previously said, we have done an energy calibration of the position spectra for the ^{114}Sn target [e.g., Fig. 1(c), α] and for the Sn$_{\mathrm{nat}}$ target [e.g., Fig. 1(c), β] of each magnetic field setting by means of the measured ^{116}Sn(p,t)^{114}Sn spectra. Starting from the Fig. 1(c) α calibrated spectrum, properly subtracting the Fig. 1(c) β calibrated spectrum, i.e., taking into account also the contaminant isotope percentage ratio between ^{114}Sn and Sn$_{\mathrm{nat}}$ targets, we have obtained the "clean" ^{112}Sn energy spectrum of Fig. 1(c) γ. We have followed this procedure for every angle and every magnetic setting, in order to obtain the correct angular distribution cross-section for each identified level.

As a check of the correctness and of the reliability of the adopted procedure we have also reconstructed angular distributions for the contaminants. In Fig. 2 the differential cross sections for the contaminant levels identified in Fig. 1(c) α are shown. Figure 3 shows the differential cross section for the ^{112}Sn(p,t)^{110}Sn as reconstructed from the Sn$_{\mathrm{nat}}$ target collected spectra. It has to be noted that the ^{112}Sn abundance in the natural tin is 1%.

We have studied 28 (p,t) transitions (including one doublet) to the final states of ^{112}Sn up to $E_x = 3.624$ MeV. The spins and parities of all the 29 levels of ^{112}Sn have been assigned by the DWBA analysis reported in Sec. II B.

Table II summarizes the results obtained in the present experiment. The energies, spins, and parities of the ^{112}Sn levels adopted previously [8] are listed together with the energies, spins, and parities observed in the present study of the ^{114}Sn(p,t)^{112}Sn reaction. The integrated cross sections, estimated with a systematic error of 30%, are also reported in the last column of Table II, together with their statistical errors.

B. Cluster DWBA analysis

In order to assign the value of the transferred angular momentum and spin for each level in the final nucleus ^{112}Sn, we have compared the experimental angular distributions with the predictions of cluster DWBA calculations.

A direct one-step (p,t) transfer reaction on an even-even 0^+ target nucleus populates only natural parity states of the residual nucleus, with a unique L transfer, if we assume that the two neutrons are transferred in a singlet ($S = 0$) state, with relative orbital angular momentum zero. With this assumption, the J^π of the observed levels are directly and unambiguously given by the assignment of the L transfer $[J_f = L, \pi_f = (-1)^L]$.

DWBA analyses of the differential cross sections for the ^{114}Sn(p,t)^{112}Sn reaction have been carried out assuming a semimicroscopic dineutron cluster pickup. Our DWBA analysis is along the same lines of those performed in the case of ^{112,116,118,120,122,124}Sn(p,t)^{110,114,116,118,120,122}Sn [1–5], with the basic assumption that the relative motion of the transferred spin-singlet neutron pair has zero angular momentum and no radial nodes. A single-particle wave function with angular momentum equal to the angular momentum L of the transferred neutron pair describes the center-of-mass wave function of the transferred pair. The radial dependence of the center-of-mass wave function is obtained by solving the radial Schrödinger equation for the dineutron requiring that the number of radial nodes N is given by the conservation law for three-dimensional harmonic oscillator quanta:

$$Q = 2N + L = \sum_{i=1}^{2}(2n_i + \ell_i),$$

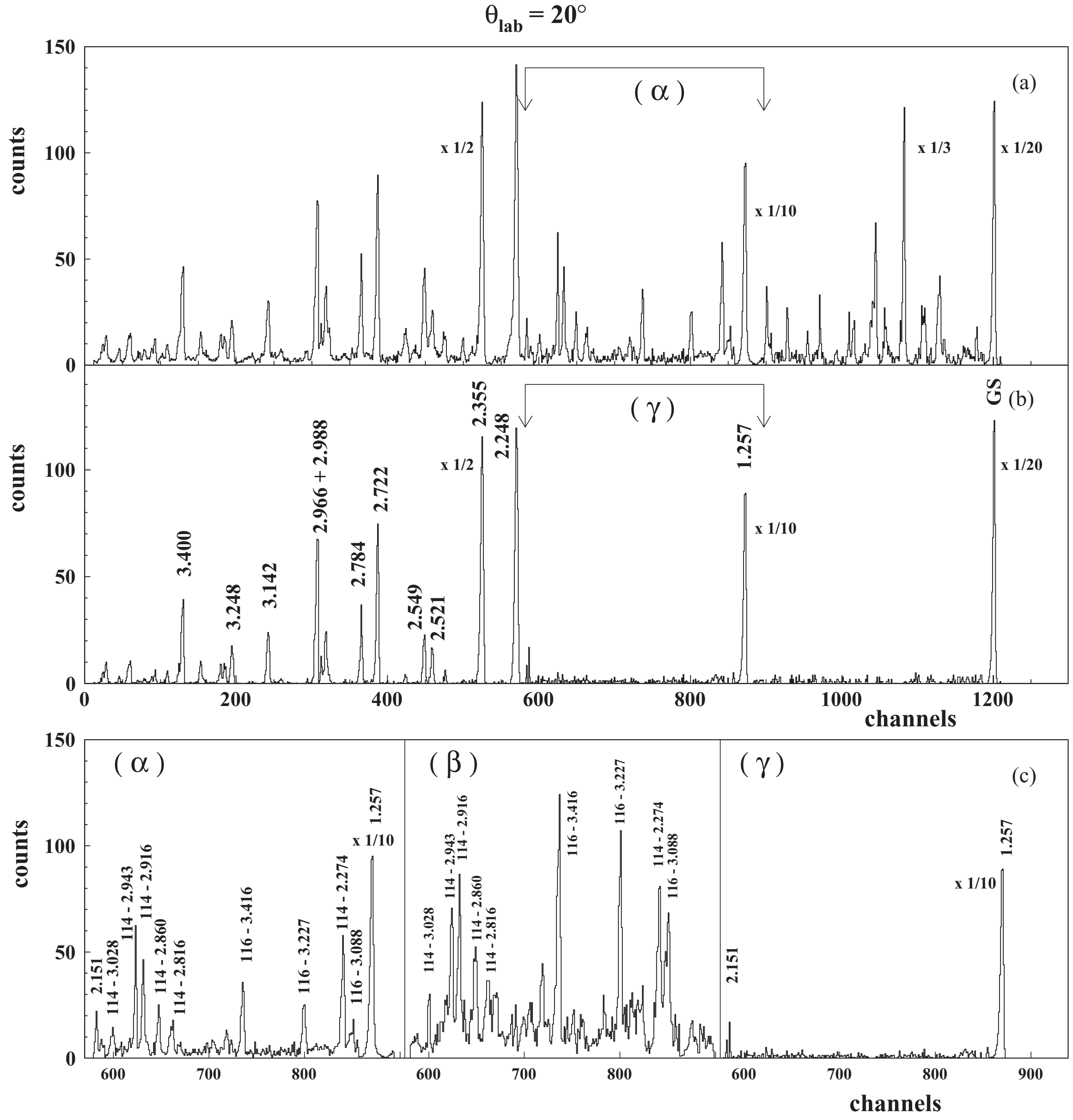

FIG. 1. Position spectra of tritons measured at $\theta = 20^\circ$. (a) Position spectrum as collected on-beam from the ^{114}Sn target at several magnetic settings. Due to the presence of the other tin isotopes in the target, many levels, coming from the (p,t) reaction on all the other tin isotopes, are visible. (b) Position spectrum of tritons showing only the transitions to the residual nucleus ^{112}Sn as obtained from the spectrum of (a), by "properly subtracting" contribution of the other tin isotopes. In both (a) and (b) the arrows (portions α and γ) indicate the part of the spectrum corresponding to the second collected magnetic setting. (c) The position spectra corresponding to the second magnetic setting of the spectra shown in (a) and (b) (α and γ, respectively) are reported, while the β spectrum is due to the tritons coming from the target of natural tin, obviously collected with the same magnetic field setting. For the sake of simplicity only some levels are labeled with their excitation energies in MeV. Except for ^{112}Sn, the residual nuclei are indicated with their mass number.

where n_i and l_i are the quantum numbers of the individual shell-model states that form the transferred pair.

The calculated angular distributions are characterized mainly by L, and are only slightly affected if N changes by one. As the shapes of the angular distributions depend very little on the detailed microscopic shell-model components of the transferred dineutron cluster, the DWBA calculations represent a valuable tool in the use of the shape of the observed angular distributions to identify the transferred angular momentum L. The detailed shell-model structure of the transferred cluster (i.e., n_i and l_i values of the cluster components and their relative phases) is very important to determine the magnitude of the transfer cross section, as will be shown in Sec. IV.

The DWBA calculations have been performed in finite-range approximation, using the computer code TWOFNR [24] and a proton-dineutron interaction potential of Gaussian form $V(r_{p2n}) = V_0 \exp[-(r_{p2n}/\xi)^2]$ with $\xi = 2$ fm. The optical model parameters for the proton entrance channel have been

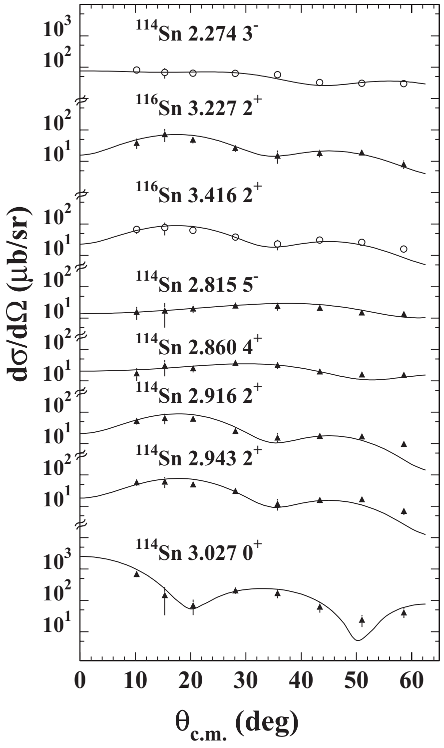

FIG. 2. Differential cross sections for the levels identified in the portion of spectrum shown in Fig. 1(c), α (second magnetic setting), as due to other tin isotopes present in the target (see text). The dots represent the experimental data, the solid lines the theoretical estimates obtained with semimicroscopic DWBA calculations.

deduced from a systematic survey of elastic scattering by Perey [25] and for the triton exit channel by Fleming *et al.* [6] and were slightly adjusted to improve the agreement with the experimental angular distributions. Table III summarizes the optical model parameters for the proton and triton elastic scattering, used in the Woods-Saxon parametrization, and the geometric parameters used for evaluating the bound-state

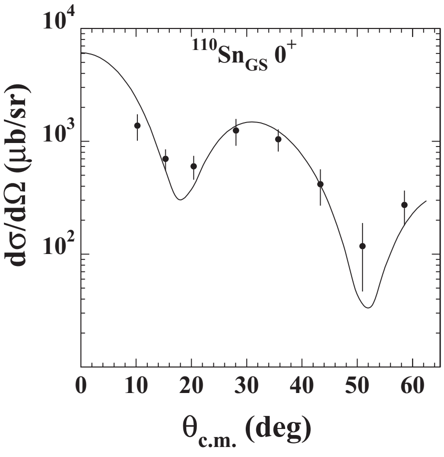

FIG. 3. Differential cross section for the ^{112}Sn$(p,t)^{110}$Sn reaction, as reconstructed from the spectrum of the natural tin target (see text). The dots represent the experimental data, the solid lines the theoretical estimates obtained with semimicroscopic DWBA calculations.

TABLE II. Columns 1 and 2 give the adopted energies, spins, and parities; columns 3 and 4 the energies, spins, and parities observed in the present work; column 5 gives the integrated cross sections from 10° to 57.5°. Our energies have an uncertainty of ±3 keV. In column 5 integrated cross sections, estimated with a systematic error of ±30%, are reported together with their statistical errors.

Adopted		Present Experiment		
$E_{\rm exc}$ (keV)	J^π	$E_{\rm exc}$ (MeV)	J^π	$\sigma_{\rm int}$ (μb)
0.0	0^+	0.000	0^+	1519.3 ± 16.2
1256.85	2^+	1.257	2^+	230.0 ± 2.9
2151.09	2^+	2.151	2^+	3.5 ± 0.7
2190.9	0^+			
2247.62	4^+	2.248	4^+	67.3 ± 5.3
2354.53	3^-	2.355	3^-	91.7 ± 6.3
2476.20	(2^+)	2.476	2^+	2.8 ± 0.7
2521.05	4^+	2.521	4^+	10.0 ± 1.9
2549.30	6^+	2.549	6^+	22.6 ± 4.3
2556.6	LE 2			
2618	0^+	2.618	0^+	2.4 ± 0.6
2721.56	2^+	2.722	2^+	24.8 ± 3.3
2756.19	$2^+,3,4^+$			
2783.92	4^+	2.784	4^+	20.2 ± 2.7
2860				
2913.4	$2^+,3^+,4^+$			
2917.71	$2^+,3^+,4^+$			
2926.78	6^+	2.927	6^+	19.0 ± 3.1
2967.00	2^+	2.966	2^+	34.0 ± 2.8
2989	0^+	2.988	0^+	41.3 ± 4.4
3078.87	$2^+,3,4^+$			
3093.07	2^+			
3118				
3137	5^-	3.142	5^-	13.3 ± 2.0
3149.41	4^+			
3248.81	2^+	3.248	2^+	8.0 ± 1.3
3278	4^+	3.275	4^+	5.8 ± 1.2
3286.39	2^+	3.286	2^+	3.5 ± 0.7
		3.345	2^+	5.8 ± 1.2
3354.43	7^-			
3384.54				
3402		3.400	4^+	20.1 ± 2.8
3414.19	6^+			
		3.414	$6^+ + 4^+$	3.7 ± 1.0
3417.77	4^+			
3430.70	8^-			
3440		3.445	4^+	2.1 ± 0.5
3456.48				
3477		3.481	4^+	2.8 ± 0.4
3502		3.510	5^-	4.0 ± 0.5
3524.79	$2^+,3,4^+$			
3530.44	$2^+,3,4^+$			
3553.98	$2^+,3^+,4^+$			
		3.554	3^-	5.7 ± 0.9
3570	0^+			
3580	4^+			
		3.586	2^+	2.3 ± 0.5
3611				
3624	(2^+)	3.624	4^+	6.3 ± 0.9

TABLE III. The Woods-Saxon optical model parameters for the incident proton, the outgoing triton, and the geometrical parameters for the bound state of the transferred dineutron cluster.

	V_r (MeV)	r_r (fm)	a_r (fm)	W_v (MeV)	r_v (fm)	a_v (fm)	W_d (MeV)	r_d (fm)	a_d (fm)	V_{so} (MeV)	r_{so} (fm)	a_{so} (fm)	r_c (fm)
p	50.0	1.25	0.65				10.0	1.30	0.60	3.00	1.25	0.70	1.25
t	176.0	1.14	0.72	18.0	1.61	0.82				8.00	1.10	0.80	1.30
BS		1.30	0.50										

wave function of the transferred dineutron cluster. The good agreement between experimental results and cluster DWBA calculations for the ^{114}Sn$(p,t)^{112}$Sn reaction suggests that the multistep processes, which are not taken into account in the present DWBA calculations, are small in this region of masses and at this bombarding energy, as already reported in the case of all the even tin isotopes studied [1–5].

We have assigned the transferred L values and consequently spins and parities of levels of the residual nucleus ^{112}Sn by means of the comparison between the shapes of the experimental angular distributions and the calculated ones, owing to their pronounced structure and difference for different L transfers. The 0^+ states are in Fig. 4; the 2^+ states are in Fig. 5; the 4^+ states are in Fig. 6; the 6^+ states and the doublet at 3.414 MeV are in Fig. 7; the 3^- and 5^- states in Fig. 8. In these figures the angular distributions for the observed levels are compared with the cluster DWBA calculations. For the doublet, the percentages of the two different L contributions have been determined minimizing the χ^2 of the fit to the angular distribution.

C. Spin and parity assignment

As reported in Table II, we have made spin and parity assignments for all the observed levels. In particular 3 levels have been observed for the first time and identified in J^π. With respect to the adopted levels (NDS) [8], 18 assignments

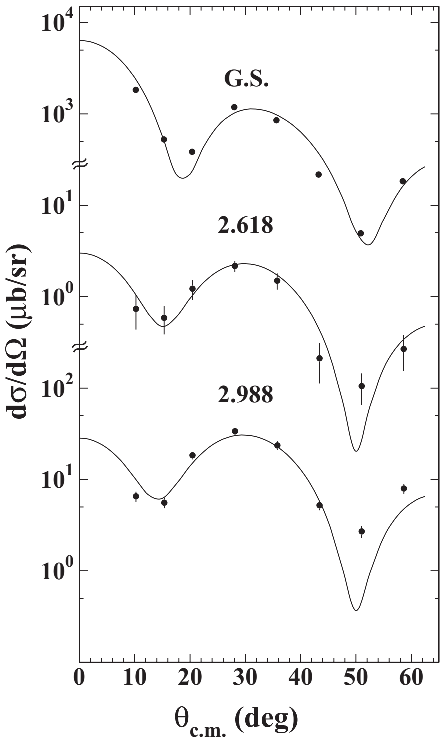

FIG. 4. Differential cross sections for the excitation of 0^+ states by the ^{114}Sn$(p,t)^{112}$Sn reaction. The dots represent the experimental data, the solid lines the theoretical estimates obtained with semimicroscopic DWBA calculations. The energies attributed to the observed levels are those given in the present work.

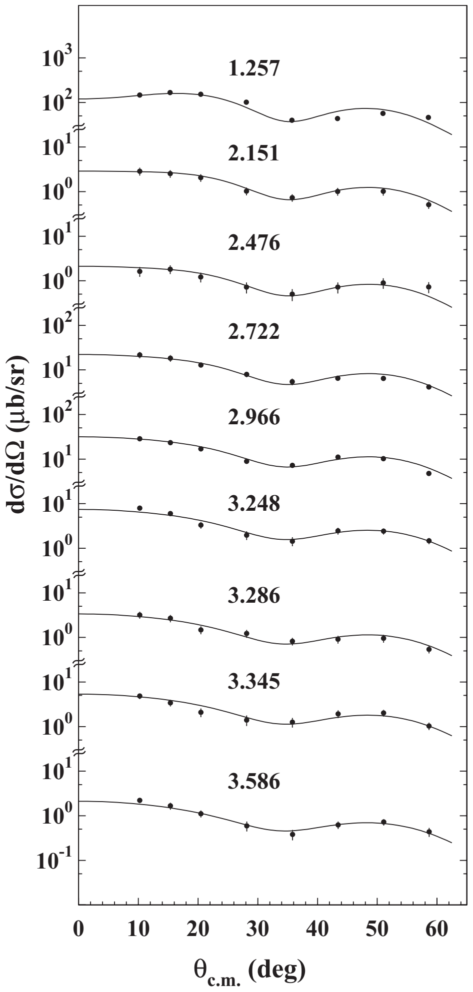

FIG. 5. Differential cross sections for the excitation of 2^+ states by the ^{114}Sn$(p,t)^{112}$Sn reaction. The dots represent the experimental data, the solid lines the theoretical estimates obtained with cluster DWBA calculations. The energies attributed to the observed levels are those given in the present work.

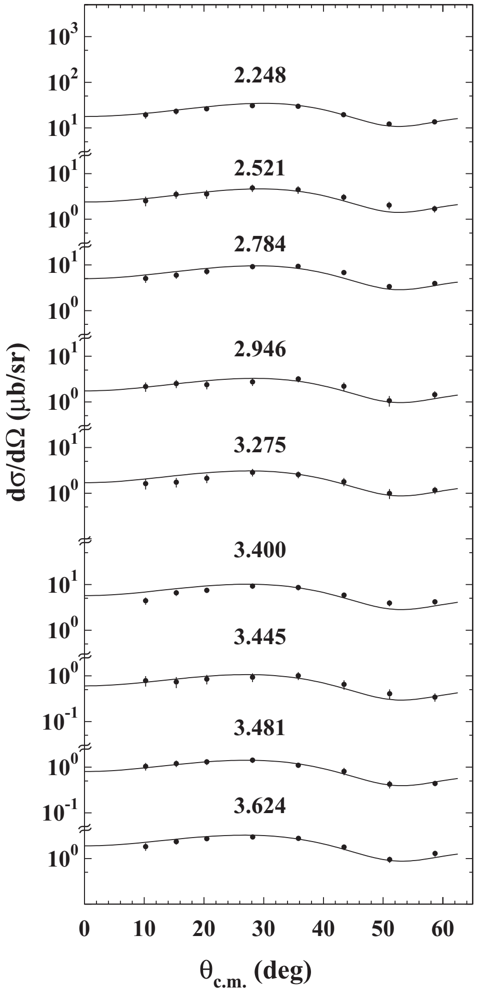

FIG. 6. Differential cross sections for the excitation of 4^+ states by the ^{114}Sn$(p,t)^{112}$Sn reaction. The dots represent the experimental data, the solid lines the theoretical estimates obtained with cluster DWBA calculations. The energies attributed to the observed levels are those given in the present work.

have been confirmed, 2 ambiguities removed, and 4 new assignments proposed. One unresolved doublet has been observed, giving 2 confirmations.

In the following we propose assignments for those levels observed in the present experiment that were not previously observed or that are reported in NDS [8] with uncertain or without J^π assignment. Assignments are also proposed for the unresolved doublet.

2.476 MeV. The NDS [8] compilation reports a level at 2476.20 keV, deduced from ^{112}Sn ϵ decay (51.4 s) [9] and from (p,p') [18] studies, with tentative (2^+) spin and parity assignment. This level was not observed in the ^{110}Cd$(\alpha,2n\gamma)^{112}$Sn [14]. The observed level is weakly excited in our experiment and the angular distribution is quite well reproduced by assuming an $L = 2$ transfer. The present assignment of $J^\pi = 2^+$ removes the uncertainty in the NDS assignment.

3.345 MeV. At this energy, the adopted level scheme [8] gives no level. The observed level is weakly populated in our experiment and is consistent with an attribution of 2^+.

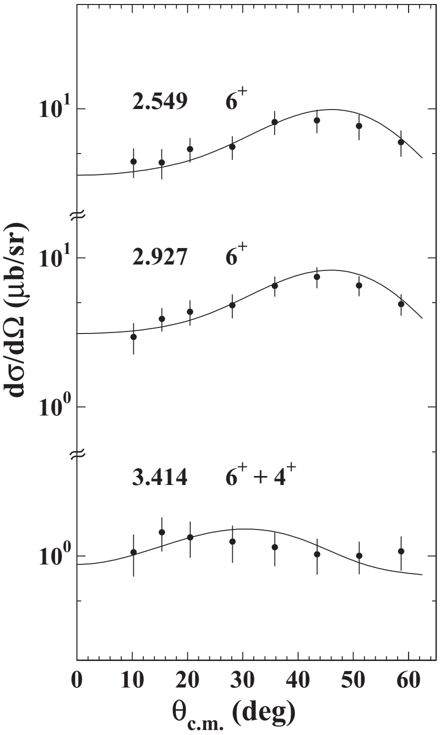

FIG. 7. Differential cross sections for the excitation of 6^+ states and one doublet [6^+ (40%) + 4^+ (60%)] at 3.414 MeV by the ^{114}Sn$(p,t)^{112}$Sn reaction. The dots represent the experimental data, the solid lines the theoretical estimates obtained with cluster DWBA calculations. The energies attributed to the observed levels are those given in the present work.

3.400 MeV. The adopted level scheme [8] reports a level without spin and parity attribution at 3402 keV, observed in the ^{112}Sn(p,p') reaction. In the present experiment the angular distribution of the tritons populating the level at 3.400 MeV is well reproduced by an $L = 4$ transfer. The present attribution is therefore $J^\pi = 4^+$.

3.414 MeV. The NDS [8] report two levels with energies 3414.19 keV and 3417.77 keV with $J^\pi = 6^+$ and 4^+, respectively. The first one was identified in ^{110}Cd$(\alpha,2n\gamma)^{112}$Sn [15] and the second one from the ^{112}Sn ϵ decay (51.4 s) [9] and from (p,p') [18]. The J^π of the second level is assigned on the basis of the L transfer from the (p,p') reaction. Our measured angular distribution is well reproduced by assuming that this transition at 3.414 MeV corresponds to an unresolved doublet of one level with $J^\pi = 6^+$ ($L = 6$ transfer, 40%) and another level with $J^\pi = 4^+$ ($L = 4$ transfer, 60%).

3.445 MeV, 3.481 MeV, 3.510 MeV. The NDS [8] report three levels at 3440 keV, 3477 keV, and 3502 keV, without spin and parity attribution, derived from a ^{112}Sn(p,p') reaction measurement [18], with a 7 keV error in the excitation energy value. A level at 3.478 MeV was also identified in the ^{114}Sn$(p,t)^{112}$Sn reaction [7] without L-transfer assignment. In our measurement the differential cross sections for the levels at 3.445 MeV, 3.481 MeV, and 3.510 MeV, corresponding to the NDS levels at 3440 keV, 3477 keV, and 3502 keV, respectively, are nicely reproduced by assuming $L = 4$, 4,

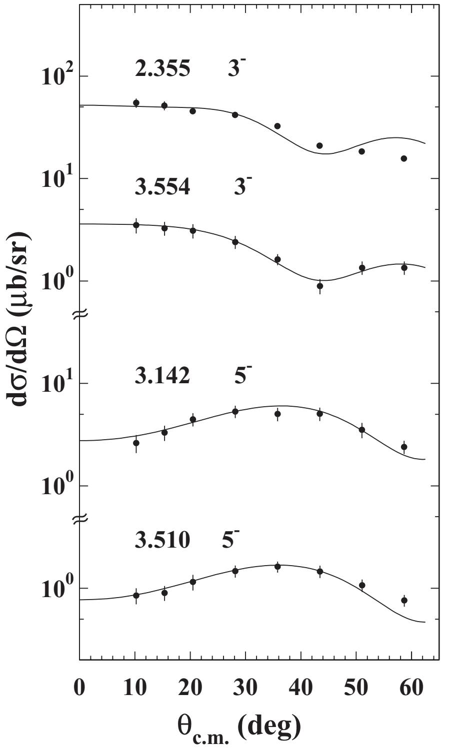

FIG. 8. Differential cross sections for the excitation of 3^- and 5^- states by the ^{114}Sn(p,t)^{112}Sn reaction. The dots represent the experimental data, the solid lines the theoretical estimates obtained with cluster DWBA calculations. The energies attributed to the observed levels are those given in the present work.

and 5, respectively. The present assignments are therefore $J^\pi = 4^+, 4^+$, and 5^-, respectively.

3.554 MeV. In the adopted level scheme [8] a level at 3553.98 keV with $J^\pi = 2^+$, 3^+, 4^+ is reported. The J^π assignment is inferred from the allowed β transition from the 3^+ state of ^{112}Sb. In the present study, an $L = 3$ transfer quite well reproduces the angular distribution. The present assignment is therefore $J^\pi = 3^-$. The level we find at 3.554 MeV does not coincide with the adopted 3553.98 keV level.

3.586 MeV. The shape of the angular distribution of this quite weakly populated level is consistent with an attribution of $J^\pi = 2^+$. This level cannot correspond to the adopted level [8] reported at (3580 ±5) keV with $J^\pi = 4^+$ inferred from a study of the ^{112}Sn(p,p') reaction [18].

3.624 MeV. The NDS [8] report a level at 3624 keV with a tentative $J^\pi = (2^+)$ from a ^{112}Sn(p,p') reaction study [18], which assumes an $L = (2)$ transfer. In our measurement we reproduce quite well the differential cross section by assuming an $L = 4$ transfer. The present assignment $J^\pi = 4^+$ removes the uncertainty in the NDS assignment.

III. SHELL-MODEL CALCULATIONS AND COMPARISON WITH THE EXPERIMENTAL ENERGY SPECTRUM

In this section, we compare the excitation energies obtained from a realistic shell-model calculation with those of the present experiment. This calculation, in which we assume ^{100}Sn as closed core and let the 12 valence neutrons occupy the five levels $0g_{7/2}$, $1d_{5/2}$, $1d_{3/2}$, $2s_{1/2}$, and $0h_{11/2}$ of the 50-82 shell, is performed along the same lines as those of our previous studies on the ^{110,114,116,118,120,122,124}Sn isotopes [1–5]. In particular, the shell-model Hamiltonian is the same we used in Ref. [1] for ^{110}Sn. For the sake of completeness, we report here the adopted single-particle energies (in MeV): $\epsilon_{g_{7/2}} = 0.0$, $\epsilon_{d_{5/2}} = 0.01$, $\epsilon_{s_{1/2}} = 2, 2$, $\epsilon_{d_{3/2}} = 2, 3$, and $\epsilon_{h_{11/2}} = 3.25$. We refer to [1] for details about this choice. As regards the matrix elements of our effective interaction, we only mention that they are constructed by means of the so-called $\hat{Q}$-box folded-diagram method with a low-momentum potential $V_{\text{low-k}}$ [26] derived from the CD-Bonn free nucleon-nucleon potential [20]. Note that the excitation energies presented in this section are obtained by performing full shell-model calculations using the OSLO code [27], while the two-nucleon transfer amplitudes, needed as input for the theoretical cross-section angular distributions (see next section), have been computed within the framework of the seniority scheme truncating the model space to states with seniority $v \leqslant 4$. The matrix elements of the two-particle transfer operator between wave functions of ^{112}Sn states and the ^{114}Sn ground state are obtained, as in all our previous calculations for tin isotopes, from the chain-calculation method described in Refs. [4,28].

TABLE IV. Comparison of calculated energies for ^{112}Sn with those obtained from the present experiment. See text for details.

J^π	E_{expt} (MeV)	E_{calc} (MeV)	J^π	E_{expt} (MeV)	E_{calc} (MeV)
0^+	0.000	0.000	6^+	2.549	2.587
	2.618	2.441		2.927	2.860
	2.988	2.937		3.414	3.912
2^+	1.261	1.920	3^-	2.335	3.290
	2.151	2.439		3.554	3.592
	2.476	2.902			
	2.722	3.022	5^-	3.142	3.283
	2.966	3.223		3.510	3.570
	3.248	3.245			
	3.286	3.406			
	3.345	3.595			
	3.586	3.681			
4^+	2.248	2.326			
	2.521	2.594			
	2.784	2.933			
	2.946	3.072			
	3.275	3.222			
	3.400	3.478			
	3.414	3.815			
	3.445	3.925			
	3.481	3.992			
	3.624	4.139			

The calculated excitation energies of ^{112}Sn are compared with the experimental ones in Table IV. A further important test of the wave functions, in particular as regards the role of components outside the chosen model space, is provided by the analysis of the differential cross sections, which will be discussed in the next section. Note that our energies are eigenvalues of an effective Hamiltonian, whereas in the calculation of the spectroscopic amplitudes we have just used a bare operator. This means that the former account perturbatively for excitations not explicitly included in our model space, while this is not the case for the latter.

From Table IV we see that the two observed 0^+ excited states, as well as the 4^+ and 6^+ states below 3.4 MeV, are very well reproduced by our calculations. In fact, the discrepancies range from a few tens of keV to at most 180 keV for the first 0^+ excited state. The third 6^+ state as well as the other four 4^+ states are predicted to lie at about 500 keV above the experimental ones. The latter are just shifted as a whole.

We now come to the 2^+ states. First, we see that the energy of the first 2^+ state is significantly overestimated by the theory, which is, however, a feature of our shell-model description of tin isotopes. In fact, we have met the same problem in our previous calculations for light tin isotopes [29] and ^{110,114}Sn [1,2]. This may be related to possible proton-core excitations, which have been proposed as an explanation of the observed excess in the $B(E2; 2^+ \rightarrow 0^+_{\text{gs}})$ strength in the Sn isotopes [30]. Eight other 2^+ levels have been populated in the present experiment in the energy interval 2.1–3.6 MeV. The same number of states is predicted by the theory between 2.4 and 3.7 MeV. However, when we try to establish a one-to-one correspondence between the observed and calculated levels, it turns out that the discrepancies do not show a regular behavior as is the case for the 4^+ states. Indeed, we see that the second and third 2^+ states are overestimated by about 300 and 400 keV, respectively, while for the other states the discrepancy oscillates from a few keV up to about 300 keV.

As for the negative parity states, only two 3^- and two 5^- levels have been observed and their excitation energies are well reproduced by our calculations, except that of the first 3^- level which is overestimated by about 1 MeV. This very large difference may be explained by considering that a substantial contribution from particle-hole excitations, that are outside our model space, is likely to enter the description of the yrast 3^- state. On the other hand, we cannot exclude, as discussed in [1] for ^{110}Sn, that this state has no theoretical counterpart. Should this be the case, our first 3^- state would be identified with the second observed one, the difference between their excitation energies being only about 250 keV.

IV. MICROSCOPIC DWBA CALCULATIONS

A comparison of the observed ^{112}Sn energy levels with the predictions of a microscopic shell-model calculation has been presented in the previous section. Now we will compare the measured ^{114}Sn$(p,t)^{112}$Sn differential cross sections with those calculated from the ^{114}Sn and ^{112}Sn shell-model eigenstates. The theory underlying the microscopic calculation of the differential cross sections has been presented elsewhere [31,32]. The essential physical assumption is that the (p,t) reaction is direct, only involving the degrees of freedom of the proton and the two transferred neutrons. Because an exact treatment of the interaction between the proton and the two neutrons in the field provided by the ^{112}Sn core is not available, we make the usual approximation that the transfer does not change the relative motion of the two neutrons. Thus the ^{112}Sn final states that are most strongly populated are those whose wave functions differ from the ^{114}Sn ground state by two neutrons with relative motion similar to the relative motion of the two neutrons in the triton. These triton neutrons have zero relative angular momentum, and total spin zero (predominantly). This is similar to the motion associated with pairing correlations in nuclei. Thus the states that are most strongly populated in ^{114}Sn$(p,t)^{112}$Sn are the states lowest in excitation energy, which are the states that have been most strongly affected by the attractive pairing component of the internucleon force.

A more complete calculation of the (p,t) reaction between tin isotopes has been performed by Potel *et al.* [33]. It uses the detailed interaction between the proton and the transferred neutrons, and takes account of the contributions of successive and simultaneous transfer of the neutrons. It successfully accounts for the absolute values of the differential cross sections. However, these more detailed calculations were restricted to transitions to states of zero angular momentum, which are only a very small fraction of the final ^{112}Sn states studied in this work.

Because of the simplifications implicit in our reaction theory, our calculated differential cross sections are undetermined by an overall factor. Its value should be independent of the final ^{112}Sn state, and the angle of the outgoing triton. For convenience, we choose this overall factor to provide the best visual fit to the ground-state transition. The shapes of the angular distributions are determined mostly by the angular momentum transferred along with the transferred nucleons, and by the geometry and strengths of the optical potentials in which the proton and triton potential move. As can be seen in Figs. 9 to 13, the theory gives a very good description of the observed shapes, which allows for a relatively unambiguous comparison between the magnitudes of the observed and calculated differential cross sections. This provides a rather severe test of our calculated eigenstates. The shell-model description of the wave function of the transferred neutrons involves a coherent combination of coupled two-neutron shell-model states. Because of this coherence, the calculated differential cross section is strongly dependent on the relative phases of the component two-neutron states, and unless the calculation gets them right, the attempt to explain the data will fail. Furthermore, since the transfer reaction occurs mainly in the vicinity of the nuclear surface, the calculated differential cross sections will be strongly dependent on the surface magnitudes of the single-particle neutron wave functions, which are different for different single-particle states. Thus it is also important for the calculation to identify the dominant single-particle states associated with the transition to each ^{112}Sn final state. In summary, the fit to the magnitude of the ground-state differential cross section is chosen to fix the overall normalization of the calculated results; once this is done, the comparison between the observed and calculated differential cross sections of all other states is a test of the accuracy of the calculated shell-model eigenstates.

A. 0^+ transitions

It is seen from Fig. 9 that the shell-model eigenvectors give a very good account of the relative populations of the three 0^+

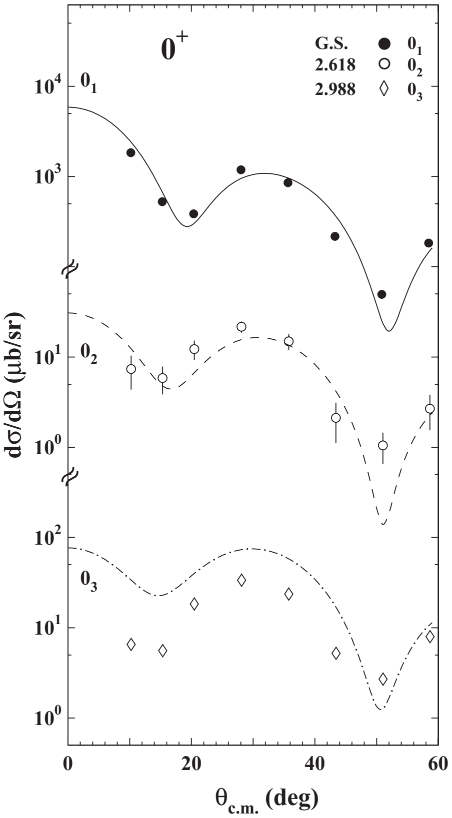

FIG. 9. Comparison between experimental and calculated cross sections for 0^+ of ^{112}Sn. The lines represent results of the microscopic calculations of the differential cross sections (in μb/sr) as a function of center-of-mass angle (in degrees). The subscripts 1,... associated with the lines indicate the calculated energy ranking of the corresponding state, with 1 representing the lowest state of given J^π. The error bars associated with the points are smaller than the symbols used to represent the points.

levels. At 28°, the measured differential cross sections are in the ratios 1185/2.2/34, compared to the calculated differential cross section ratios of 949/1.6/73, respectively. The great relative strength of the ground transition is well accounted for by the larger pairing component in the ^{112}Sn ground-state eigenvector.

B. 2^+ transitions

Figure 10 shows that the 2^+ measured differential cross sections are also reproduced by predictions based on their respective shell-model eigenvectors, with the exception of the transitions to the 2^+ levels at 2151 and 2476 keV. The theory overpredicts these differential cross sections by factors of about 20 and 30, respectively. Evidently, these two levels have appreciable shell-model components that cannot be reached by (p,t) pickup from the ^{114}Sn ground state. For example, if the ^{114}Sn ground state has filled $Z = 50$ proton shells, as we have assumed, the 2151 keV and 2476 keV levels would not be populated in $^{114}\text{Sn}(p,t)^{112}\text{Sn}$ if they had appreciable components with protons excited out of the $Z = 50$ proton shells.

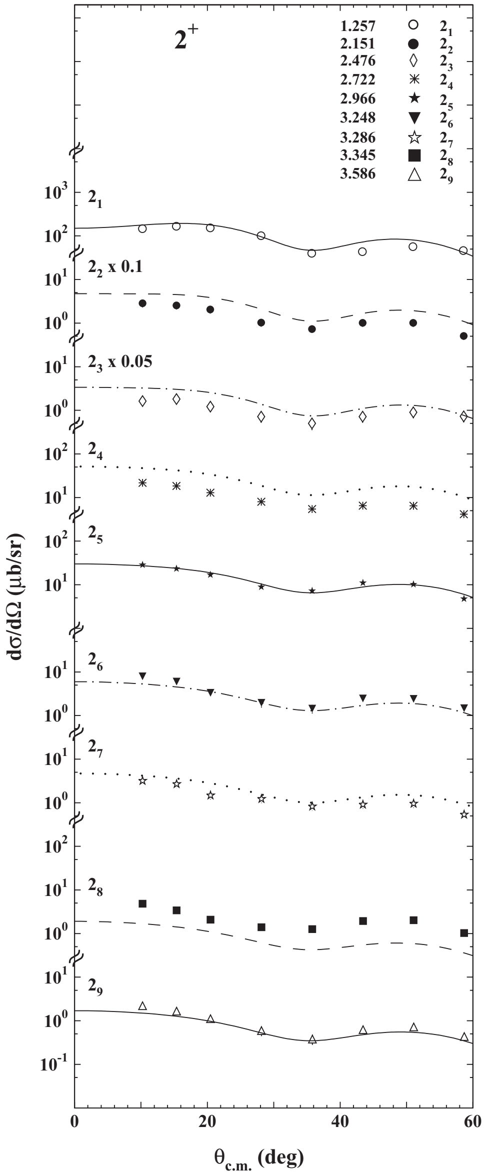

FIG. 10. Comparison between experimental and calculated cross sections for 2^+ final states of ^{112}Sn. The lines represent results of the microscopic calculations of the differential cross sections (in μb/sr) as a function of center-of-mass angle (in degrees). The subscripts 1,... associated with the lines indicate the calculated energy ranking of the corresponding state, with 1 representing the lowest state of given J^π. The error bars associated with the points are smaller than the symbols used to represent the points.

C. 4^+ transitions

Figure 11 shows that the population of the lowest three 4^+ levels is accounted for fairly well by our calculations. However, our calculations do not account for the higher 4^+ levels. For example, we strongly overpredict the population of 4_5^+ at 3275 keV, again perhaps because the real 4_5^+ level has a more complicated proton structure than we have assumed. And we strongly underpredict the population of 4_4^+, 4_8^+, and 4_9^+. This may suggest that these levels have important shell-model

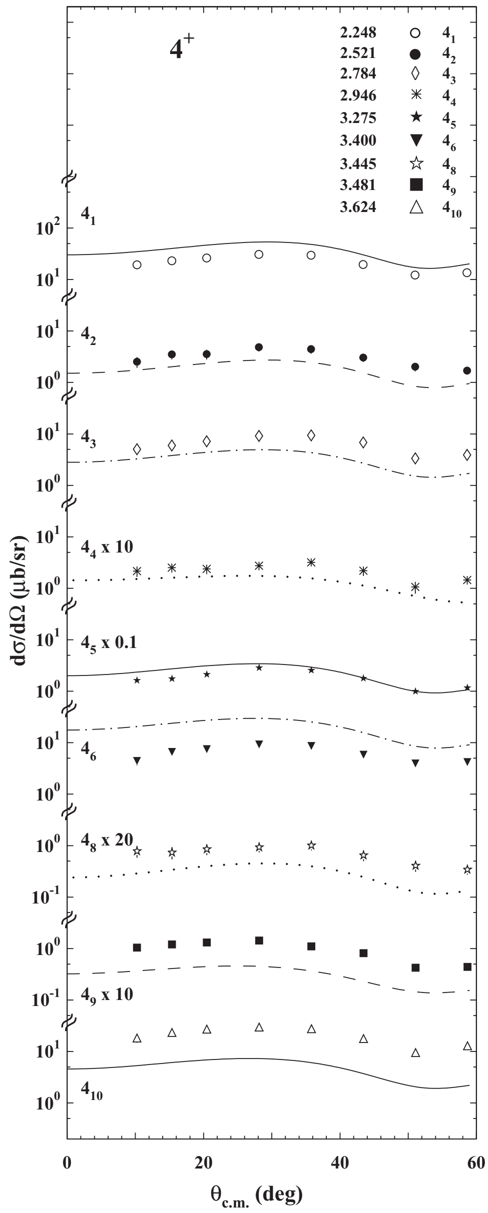

FIG. 11. Comparison between experimental and calculated cross sections for 4^+ final states of ^{112}Sn. The lines represent results of the microscopic calculations of the differential cross sections (in μb/sr) as a function of center-of-mass angle (in degrees). The subscripts 1,. . . associated with the lines indicate the calculated energy ranking of the corresponding state, with 1 representing the lowest state of given J^π. The error bars associated with the points are smaller than the symbols used to represent the points. Note that the data points correspond only to clearly resolved states. The doublet is not represented in the figure.

components involving higher-energy neutron single-particle states, not included in our calculation.

D. 6^+ transitions

Figure 12 shows that the differential cross sections for the population of the 6^+ levels at 2549 keV and 2927 keV are fairly well described by our theory. At 28°, these differential

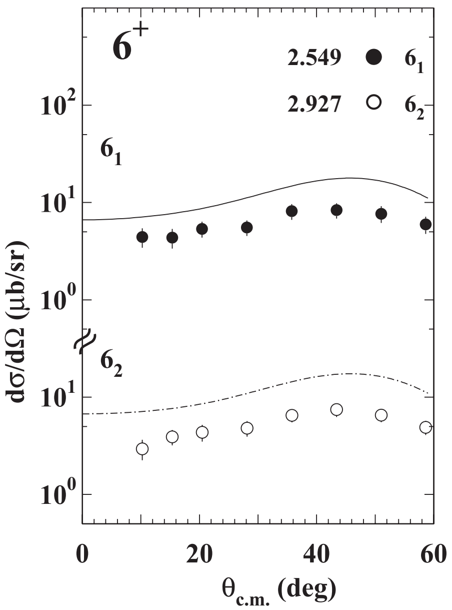

FIG. 12. Comparison between experimental and calculated cross sections for 6^+ final states of ^{112}Sn. The lines represent results of the microscopic calculations of the differential cross sections (in μb/sr) as a function of center-of-mass angle (in degrees). The subscripts 1,. . . associated with the lines indicate the calculated energy ranking of the corresponding state, with 1 representing the lowest state of given J^π. Note that the data points correspond only to clearly resolved states. The doublet is not represented in the figure.

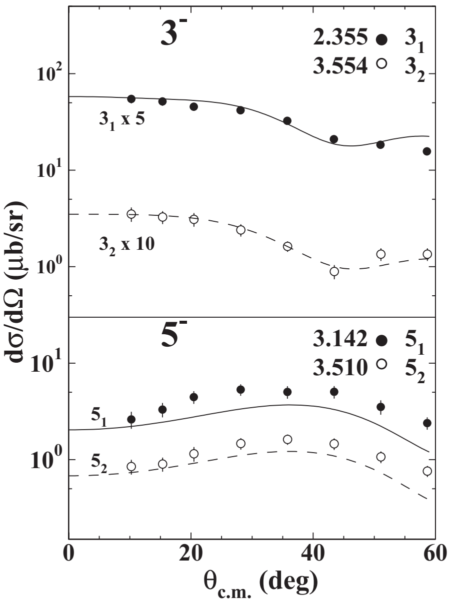

FIG. 13. Comparison between experimental and calculated cross sections for 3^-, 5^- final states of ^{112}Sn. The lines represent results of the microscopic calculations of the differential cross sections (in μb/sr) as a function of center-of-mass angle (in degrees). The subscripts 1,. . . associated with the lines indicate the calculated energy ranking of the corresponding state, with 1 representing the lowest state of given J^π. Error bars are shown for 3_2^- and 5_1^- and 5_2^- states; for 3_1^- the error bars are smaller than the symbols representing the measured differential cross sections.

cross sections are measured to be approximately 240 times weaker than the ground-state transition. Our theory has them approximately 100 times weaker.

E. 3^-, 5^- transitions

Figure 13 shows that the calculated 3^- differential cross sections strongly underpredict the measured ones. This is probably because angular momentum and parity conservation allows us only two 2-neutron contributions to 3^- transfer, namely $[h_{11/2}g_{7/2}]_{3^-}$ and $[h_{11/2}d_{5/2}]_{3^-}$. If we had included more of the odd-parity, $N = 5$ single-neutron states in the calculation, we would have had more 2-neutron contributions adding coherently to the transfer amplitude, probably resulting in increased differential cross sections. The situation is not as extreme in the case of the 5^- states, because here angular momentum and parity conservation allows us to include four 2-neutron components, $[h_{11/2}g_{7/2}]_{5^-}$, $[h_{11/2}d_{5/2}]_{5^-}$, $[h_{11/2}d_{3/2}]_{5^-}$, and $[h_{11/2}s_{1/2}]_{5^-}$. Although we slightly underpredict the 5^- differential cross sections, the error is much smaller, indicating that these four 2-neutron components comprise most of the transition amplitudes.

V. SUMMARY

The $^{114}\mathrm{Sn}(p,t)^{112}\mathrm{Sn}$ reaction has been studied in a high resolution experiment at an incident proton energy of 22 MeV. Cross-section angular distributions for 28 transitions to levels of ^{112}Sn, including one doublet, have been measured up to an excitation energy of 3.624 MeV. The spins and parities for all the observed 29 levels have been assigned by a DWBA analysis, assuming a semimicroscopic dineutron cluster pickup mechanism. The calculations have been performed in finite-range approximation.

With respect to the adopted levels, 3 levels have been observed for the first time and identified in J^π, 18 assignments have been confirmed, 2 ambiguities removed, and 4 new assignments proposed. One unresolved doublet has been observed, giving two confirmations.

In addition to the experimental work, we have carried out a shell-model study of ^{112}Sn using a two-body effective interaction derived from the CD-Bonn nucleon-nucleon potential.

As regards the energy spectrum, while for some states the discrepancies are rather large, say about 0.5 MeV, the agreement between the calculated and experimental energies may be considered remarkably good on the whole, if one keeps in mind that it comes out from a shell-model description in terms of only the valence neutron degrees of freedom. The results for ^{112}Sn presented here are completely in line with those of our previous studies [1–5] on even-mass Sn isotopes, confirming that the shell model is the main key to the understanding of this long isotopic chain. In this context, it should be emphasized that our realistic effective interaction contains no adjustable parameters. It is also worth noting that, while we have used different sets of single-particle energies for the heavier isotopes, the Hamiltonian for ^{112}Sn is precisely the same as that used for ^{110}Sn.

A zero-range one-step microscopic DWBA calculation of differential cross sections has also been performed, where we have used two-neutron spectroscopic amplitudes obtained from shell-model wave functions for ^{112}Sn and ^{114}Sn, calculated in a seniority space truncated at $v = 4$. These shell-model spectroscopic amplitudes, used in a simple one-step zero-range microscopic analysis, yield a good account of the observed populations of all the levels, with the exception of the 2_2^+ and 2_3^+ levels and the 3^- levels. The most likely explanation is that these few levels cannot be understood simply in terms of a ^{100}Sn core plus valence neutrons, but involve more complicated configurations, such as proton excitations. This illustrates that one of the advantages of the (p,t) reaction is its sensitivity to the microscopic structures of the initial and final states.

[1] P. Guazzoni, L. Zetta, A. Covello, A. Gargano, B. F. Bayman, G. Graw, R. Hertenberger, H.-F. Wirth, and M. Jaskóla, Phys. Rev. C **74**, 054605 (2006).

[2] P. Guazzoni, L. Zetta, A. Covello, A. Gargano, G. Graw, R. Hertenberger, H.-F. Wirth, and M. Jaskóla, Phys. Rev. C **69**, 024619 (2004).

[3] P. Guazzoni, L. Zetta, A. Covello, A. Gargano, B. F. Bayman, T. Faestermann, G. Graw, R. Hertenberger, H.-F. Wirth, and M. Jaskóla, Phys. Rev. C **78**, 064608 (2008).

[4] P. Guazzoni, M. Jaskóla, L. Zetta, A. Covello, A. Gargano, Y. Eisermann, G. Graw, R. Hertenberger, A. Metz, F. Nuoffer, and G. Staudt, Phys. Rev. C **60**, 054603 (1999).

[5] P. Guazzoni, L. Zetta, A. Covello, A. Gargano, B. F. Bayman, T. Faestermann, G. Graw, R. Hertenberger, H.-F. Wirth, and M. Jaskóla, Phys. Rev. C **83**, 044614 (2011).

[6] D. G. Fleming, M. Blann, H. W. Fulbright, and J. A. Robbins, Nucl. Phys. A **157**, 1 (1970).

[7] P. J. Blankert, Ph.D. thesis, Free University, Amsterdam, 1979.

[8] D. De Frenne and E. Jacobs, Nucl. Data Sheets **79**, 639 (1996).

[9] M. E. J. Wigmans, R. J. Heynis, P. M. A. van der Kam, and H. Verheul, Phys. Rev. C **14**, 229 (1976).

[10] H. Harada, T. Murakami, K. Yoshida, J. Kasagi, T. Inamura, and T. Kubo, Phys. Lett. B **207**, 17 (1988).

[11] J. Kasagi, H. Harada, T. Murakami, K. Yoshida, H. Tachibanaki, and T. Inamura, Phys. Lett. B **176**, 307 (1986).

[12] H. W. Fielding, R. E. Anderson, C. D. Zafiratos, D. A. Lind, F. E. Cecil, H. H. Wieman, and W. P. Alford, Nucl. Phys. A **281**, 389 (1977).

[13] W. Andrejtscheff, L. K. Kostov, P. Petrov, Y. Sy Savane, Ch. Stoyanov, P. von Brentano, J. Eberth, R. Reinhardt, and K. O. Zell, Nucl. Phys. A **505**, 397 (1989).

[14] J. Bron, W. H. A. Hesselink, A. van Poelgeest, J. J. A. Zalmstra, M. J. Uitzinger, H. Verheul, K. Heyde, M. Waroquier, H. Vincx, and P. van Isacker, Nucl. Phys. A **318**, 335 (1979).

[15] A. van Poelgeest, J. Bron, W. H. Hesselink, K. Allaart, J. J. A. Zalmstra, M. J. Uitzinger, and H. Verheul, Nucl. Phys. A **346**, 70 (1980).

[16] A. Bäcklin, N. G. Jonsson, R. Julin, J. Kantele, M. Luontama, A. Passoja, and T. Poikolainen, Nucl. Phys. A **351**, 490 (1981).

[17] N. G. Jonsson, A. Bäcklin, J. Kantele, R. Julin, M. Luontama, and A. Passoja, Nucl. Phys. A **371**, 333 (1981).

[18] P. J. Blankert, H. P. Blok, and J. Blok, Nucl. Phys. A **333**, 116 (1980).

[19] J. Blachot, Nucl. Data Sheets **97**, 593 (2002).

[20] R. Machleidt, Phys. Rev. C **63**, 024001 (2001).

[21] M. Loeffler, H. J. Scheerer, and H. Vonach, Nucl. Instr. Methods **111**, 1 (1973).

[22] H.-F. Wirth, H. Angerer, T. von Egidy, Y. Eisermann, G. Graw, and R. Hertenberger, in *Jahresbericht 2000, Beschleunigerlaboratorium München* (2001), p. 71.

[23] J. R. Comfort, ANL Physics Division, Informal Report PHYS-1970B, 1970 (unpublished).

[24] M. Igarashi, computer code TWOFNR, 1977 (unpublished).

[25] F. G. Perey, Phys. Rev. **131**, 745 (1963).

[26] L. Coraggio, A. Covello, A. Gargano, T. T. S. Kuo, and N. Itaco, Prog. Part. Nucl. Phys. **62**, 135 (2009), and references therein.

[27] T. Engeland, the Oslo shell-model code 1991-2006 (unpublished).

[28] A. Covello, F. Andreozzi, L. Coraggio, A. Gargano, and A. Porrino, in *Contemporary Nuclear Shell Models*, Lecture Notes in Physics Vol. 482 (Springer-Verlag, Berlin, 1997).

[29] F. Andreozzi, L. Coraggio, A. Covello, A. Gargano, T. T. S. Kuo, Z. B. Li, and A. Porrino, Phys. Rev. C **54**, 1636 (1996).

[30] R. Kumar, P. Doornenbal, A. Jhingan, R. K. Bhowmik, S. Muralithar, S. Appannababu, R. Garg, J. Gerl, M. Gorska, J. Kaur, I. Kojouharov, S. Mandal, S. Mukherjee, D. Siwal, A. Sharma, P. P. Singh, R. P. Singh, and H.-J. Wollersheim, Phys. Rev. C **81**, 024306 (2010), and references therein.

[31] B. F. Bayman and A. Kallio, Phys. Rev. **156**, 1121 (1967).

[32] D. N. Mihailidis, N. M. Hintz, A. Sethi, and E. J. Stephenson, Phys. Rev. C **64**, 054608 (2001).

[33] G. Potel, F. Barranco, F. Marini, A. Idini, E. Vigezzi, and R. A. Broglia, Phys. Rev. Lett. **107**, 092501 (2011).